Heliyon 11 (2025) e42123

Contents lists available at ScienceDirect

Heliyon

journal homepage: www.cell.com/heliyon

Research article

Landscape analysis of m6A modification reveals the dysfunction of bone metabolism in osteoporosis mice

Lifeng Zheng [a,b,1], Chao Lan [c,1], Xinyue Gao [d,1], An Zhu [d], Yaoqing Chen [a,b], Jinluan Lin [a,b], Sunjie Yan [c,e,f,g,h,i], Ximei Shen [c,e,f,g,h,i,*]

[a] Department of Orthopedics, the First Affiliated Hospital, Fujian Medical University, Fuzhou, 350005, China
[b] Department of Orthopedics, National Regional Medical Center, Binhai Campus of the First Affiliated Hospital, Fujian Medical University, Fuzhou, 350212, China
[c] Department of Endocrinology, the First Affiliated Hospital, Fujian Medical University, Fuzhou, 350005, China
[d] Key Laboratory of Gastrointestinal Cancer (Fujian Medical University), Ministry of Education, Fuzhou, 350108, China
[e] Department of Endocrinology, National Regional Medical Center, Binhai Campus of the First Affiliated Hospital, Fujian Medical University, Fuzhou, 350212, China
[f] Clinical Research Center for Metabolic Diseases of Fujian Province, the First Affiliated Hospital, Fujian Medical University, Fuzhou, 350005, China
[g] Fujian Key Laboratory of Glycolipid and Bone Mineral Metabolism, the First Affiliated Hospital, Fujian Medical University, Fuzhou, 350005, China
[h] Diabetes Research Institute of Fujian Province, the First Affiliated Hospital, Fujian Medical University, Fuzhou, 350005, China
[i] Metabolic Diseases Research Institute, the First Affiliated Hospital, Fujian Medical University, Fuzhou, 350005, China

ARTICLE INFO

Keywords:
Osteoporosis
Bone metabolism
Ovariectomy
Osteoporosis animal models
m6A methylation

ABSTRACT

Osteoporosis (OP) is a prevalent chronic bone metabolic disorder that affects the elderly population, leading to an increased susceptibility to bone fragility. Despite extensive research on the onset and progression of OP, the precise mechanisms underlying this condition remain elusive. The m6A modification, a prevalent form of chemical RNA modification, primarily regulates posttranscriptional processes, including RNA stability, splicing, and translation. Numerous studies have underscored the crucial functions of m6A regulators in OP. This study aimed to explore the relationship between OP and RNA m6A methylation, investigating its underlying mechanisms through comprehensive bioinformatic analysis and experimental validation. The mRNA sequencing (mRNA-seq) and methylated RNA immunoprecipitation sequencing (MeRIP-seq) were performed on control mice as well as ovariectomized mice to discover differentially expressed genes (DEGs) and m6A regulators in OP. The results revealed dysregulation of a majority of bone metabolism-related genes and m6A regulators in ovariectomized mice, indicating a closely linked relationship between them. Our research findings indicated that m6A modification is essential in regulating OP, offering potential insights for prevention and treatment.

Abbreviations: BMD, bone mineral density; BP, biological processes; BV/TV, bone volume fraction; CC, cellular components; Conn. D, junction density; DEGs, differentially expressed genes; GO, Gene Ontology; GSEA, gene set enrichment analysis; KEGG, Kyoto Encyclopedia of Genes and Genomes; MF, molecular functions; OP, osteoporosis; OVX, ovariectomy; PCA, principal component analysis; PPI, protein-protein interaction; SMI, structural model index; SNPs, single nucleotide polymorphisms; SNV, single nucleotide variants; Tb. N, trabecular number; Tb. Sp, trabecular separation; Tb. Th, trabecular thickness.

* Corresponding author. Department of Endocrinology, the First Affiliated Hospital, Fujian Medical University, Fuzhou, 350005, China.
E-mail address: niaoshe2006@163.com (X. Shen).

[1] These authors contributed equally to this work.

https://doi.org/10.1016/j.heliyon.2025.e42123
Received 26 September 2024; Received in revised form 19 January 2025; Accepted 19 January 2025
Available online 21 January 2025

1. Introduction

Osteoporosis (OP), a systemic metabolic skeletal disorder, is distinguished by reduced bone density, deterioration of the bone microenvironment, and heightened fragility and susceptibility to fractures, especially common among postmenopausal women [1]. Postmenopausal OP primarily stems from ovarian function decline during menopause, disrupting the balance between bone formation by osteoblasts and bone resorption by osteoclasts, resulting in systemic skeletal irregularities [2]. The prevalence of OP increases with advancing age, constituting a prominent health challenge encountered by the Chinese population aged 60 and above. Furthermore, it is anticipated to persistently surge as China's demographic undergoes aging [3]. The presence of OP and its associated complications significantly contribute to increased disability and mortality rates, thereby profoundly impacting the overall quality of life [4]. While specific pharmacological treatments for OP are currently lacking, clinical recommendations include daily intake of 800 IU vitamin D and 1000 mg calcium, engaging in regular weight-bearing exercise for 30 min three times per week, and ceasing smoking habits as preventive measures against bone loss [5]. Therefore, understanding the exact pathogenesis of OP and developing effective prevention and treatment strategies are crucial in clinical practice. Animal models serve as crucial tools in basic research and play a pivotal role throughout the process. Ovariectomy (OVX), owing to its high success rate in modeling postmenopausal OP animals, excellent reproducibility, and ability to mimic estrogen decline, has been extensively employed [6].

Normal bone mass is regulated by a dynamic interplay between bone resorption and formation. Previous studies have indicated that the disruption of this equilibrium dominated the progression of OP, particularly bone resorption due to overactivity of osteoclasts [7], and mounting evidence suggested that OP is a multifaceted disorder marked by significant heterogeneity involving genetic alterations [8]. Considered the predominant internal modification in eukaryotic cells, N6-methyladenosine (m6A) modification intricately participates in mRNA metabolism and significantly contributes to biological processes, including bone metabolic processes [9]. The dynamic and reversible nature of m6A methylation is primarily controlled by m6A methyltransferases (writers), m6A demethylases (erasers), and proteins that recognize m6A methylation (readers) [10]. RNA m6A modifications can be catalyzed by writers, including RBM15B, RBM15, METTL3, METTL5, METTL14, CBLL1, VIRMA, ZC3H13 and WTAP, which can be removed by erasers FTO and ALKBH5. Concurrently, the m6A modification can be specifically recognized by readers to regulate mRNA, including YTH-domain family proteins, insulin-like growth factor 2 mRNA-binding proteins (IGF2BP), and heterogeneous nuclear ribonucleoproteins (HNRNP) family proteins [11,12].

RNA m6A methylation has been linked to disease development, facilitating the up-regulation of oncoproteins to promote proliferation and invasion in diverse cancer cells, as well as modulating bone-related disease progression, such as osteosarcoma [13,14]. Recently, researchers have shown significant interest in the association between m6A modification and OP. For instance, a study revealed that a cluster of single nucleotide polymorphisms (SNPs) in FTO is linked to variations in bone mineral density (BMD) among Chinese populations, thereby suggesting FTO as a promising candidate for further investigation into OP [14]. METTL3 promotes osteogenesis and enhances osteogenic differentiation through the activation of the PTH/Pth1r signaling axis or PI3K-Akt signaling pathway to suppress OP [15]. Knockdown of METTL3 induces the pathological characteristics associated with OP in mice [16]. YTHDF2 can influence bone homeostasis by controlling inflammatory processes and osteoclast differentiation [17]. In addition, an increasing body of research has substantiated the impact of m6A regulators on OP. In conclusion, it is evident from the findings that m6A regulators have a pivotal effect on bone metabolism in relation to OP. Therefore, ovariectomized mice models were established to investigate the impact of m6A modification on OP progression. Finally, the effect of m6A modification on bone metabolism was further investigated through a comprehensive bioinformatics analysis and subsequent experimental validation.

2. Materials and methods

2.1. Establishment of OP animal models

12 female C57BL/6 mice (GemPharmatech Co., Ltd., China) aged 8 weeks were selected, and at 12 weeks of age, they were randomly assigned to the control group (sham operation group, n = 6) and the OVX group (n = 6), where bilateral ovaries were surgically removed to establish the OP model. The specific experimental procedures followed those outlined in a previous study [18], and mice underwent a 12-week post-OVX feeding regimen. Approval for all mouse experimental protocols and procedures were obtained from the Experimental Animal Ethical Committee of Fujian Medical University (IACUC FJMU 2022-NSFC-0201).

2.2. H&E staining and paraffin section

The tibias of mice were fixed with 4 % paraformaldehyde solution. Subsequently, the samples were treated by decalcification, dehydration, cleaning, and immersion in paraffin wax before being sectioned. According to the standardized protocol, hematoxylin and eosin (H&E) staining was conducted to investigate the structural changes in tibial bone tissue.

2.3. Micro-computed tomography (micro-CT) scan

The tibias were imaged using the SkyScan 1076 microtomography scanner at a resolution of 9 μm and subsequently evaluated utilizing microcomputed tomography. The scanning parameters were configured with 40 kV X-ray power and 0.25 mA tube current. The final image was generated by capturing three photographs at each angle (0.9°), followed by the determination of bone trabeculae

using a fixed threshold, and reconstruction of these images using NRecon software (Micro-Photonics Inc., Allentown, PA, USA). The tibial microstructural parameters were analyzed, including BMD, bone volume fraction (BV/TV), trabecular number (Tb. N), trabecular separation (Tb. Sp), trabecular thickness (Tb. Th), junction density (Conn. D), and structural model index (SMI).

2.4. High-throughput m6A MeRIP-seq and mRNA-seq

Total RNA of bone tissue was isolated using TRIzol reagent following the manufacturer's guidelines (Invitrogen, Carlsbad, CA, USA), and assessment of RNA quality was conducted based on the analysis of the 260/280 nm absorbance ratios. Poly(A) mRNA fractions were isolated using VAHTS mRNA capture beads from qualified RNA, and were cleaved into fragments ranging from 100 to 200 nt. KC-Digital Stranded mRNA Library Prep Kit for Illumina (Seqhealth, Wuhan, China) was used to prepare stranded RNA sequencing library. The library products covering 200 to 500 bps were enriched, quantified, and eventually sequenced on the Novaseq 6000 sequencer (Illumina) in the PE150 model.

2.5. Bioinformatic analysis

The raw data was processed with Trim Galore (Cambridge, UK) to clean and prepare it for analysis. Subsequently, Hisat2 was employed to align the sequencing results with the reference genome [19]. For RNA expression quantification in mRNA-seq data, StringTie (Baltimore, MD, USA) was utilized [20], while DESeq2 was applied for analyzing differential gene expression [21]. Moreover, m6A peak calling identification and differential methylation analysis were conducted using Exomepeak2 (Suzhou, China) [22]. STERME [23] was employed to ascertain the presence of consensus m6A motif sequences within the identified m6A peaks. MetaTX (Suzhou, China) [24] was used for visualizing the distribution pattern of epitranscriptome profiles. Enrichment analysis of Gene Ontology (GO), encompassing biological processes (BP), cellular components (CC), and molecular functions (MF), along with Kyoto Encyclopedia of Genes and Genomes (KEGG) pathways for differentially expressed genes (DEGs), was conducted using the DAVID database (Frederick, MD, USA) [25]. Entries were considered significantly enriched when $p < 0.05$. ConsRM (Suzhou, China) [26] and RMDisease (Suzhou, China) [27] were used to acquire the results regarding the conservation and diseases association of m6A. The starBase v2.0 (Guangzhou, China) provided substrates for m6A regulators certified by CLIP technology [28]. Visualization of m6A patterns at gene methylation sites was achieved using IGV 2.16.0 software. Functional protein-protein interaction (PPI) analysis was conducted through STRING and displayed in Cytoscape. Gene set enrichment analysis (GSEA) and heatmap plotting were carried out utilizing the Bioinformatics online tool (https://www.bioinformatics.com.cn/, accessed on 5 June 2023).

2.6. Identification of the variation levels of control and ovariectomized mice

The duplicated reads were removed by the Picard software (http://broadinstitute.github.io/picard/, accessed on 1 July 2024), and the variant sites were detected by bcftools [29] which compared with reference genome mm10. The variants type and location were annotated by the annovar [30]. The ggplot2 package in R 4.3.0. was used to analyze and visualize the annotated data.

2.7. Bone tissue protein extraction

To prepare the extract, we added 2 μl of protease inhibitor and 2 μl of protein stabilizer per 500 μl of cold bone tissue protein extract based on the sample size. The mixture was thoroughly mixed and stored at a temperature range of 2–8 °C. Fresh bone tissue samples were collected and immersed in pH 7.4 PBS buffer or normal saline at 4 °C. The solutions were refreshed, the samples were thoroughly soaked again, and then washed with distilled water to eliminate blood and red blood cells. The bone tissue was sectioned, weighed and placed in a mortar containing liquid nitrogen. Subsequently, the bone tissue was pulverized into powder to prevent complete evaporation of the liquid nitrogen. The resulting bone tissue powder was then transferred to centrifuge tubes, with 200 mg of bone tissue mixed with 500 μl protein extract per tube. The mixture was oscillated with the oscillator at a low speed at 4 °C for 30 min, and subjected to ultrasound at a power of 80 W for 10 s or ice bath ultrasound repeated ten times with intervals of 10 s. The supernatant obtained from the mixture, which was centrifuged for 10 min at 12,000 rpm and 4 °C, was then carefully transferred to another pre-cooled sterile centrifuge tube to extract the total protein from the bone tissue. These protein extracts were either directly utilized for downstream experiments or stored at −80 °C.

2.8. Western blotting

The protein concentration was determined using the bicinchoninic acid (BCA) assay. Subsequently, the proteins were separated by electrophoresis on polyacrylamide gels and transferred to membranes. The membranes were then blocked with 5 % skim milk at room temperature for 1 h, followed by overnight incubation at 4 °C with primary antibodies, namely FBXO40 (Bioss, Beijing, China, cat. number bs-16049R), TRIM63 (Proteintech, Wuhan, China, cat.number 55456-1-AP), PTX3 (Abcam, Cambridge, UK, cat.number ab90806), IGF2BP2 (Abcam, cat.number ab124930), which were used at dilutions of 1:8000, 1:3000, 1:1000, and 1:3000, respectively. β-actin (ABclonal, Wuhan, China, cat.number 20536-1-AP) was employed as internal control at a dilution of 1:10,000. Subsequently, a 90-min incubation with secondary antibodies was carried out. These secondary antibodies included horseradish peroxidase (HRP)-conjugated goat anti-rat IgG (Proteintech, cat.number SA00001-15), HRP goat anti-rabbit IgG (ABclonal, cat. number AS014), and HRP-conjugated affinipure goat anti-mouse IgG (Proteintech, cat.number SA00001-1), all at a dilution of

1:10,000. The membranes were exposed to a super-enhanced chemiluminescence (ECL) reagent (HRbio, Fujian, China), and images were captured using an Amersham Imager 680 (GE Healthcare Bio-Sciences AB, Uppsala, Sweden).

2.9. Immunohistochemical staining

The tibias of mice were collected and subjected to decalcification treatment with ethylene diamine tetraacetic acid. After being embedded in paraffin blocks, the samples were sliced to a thickness of 3 μm for subsequent immunohistochemical staining. The prepared sections were deparaffinized with xylene, rehydrated with ethanol, antigen retrieval was performed using hyaluronidase and pepsin, followed by blocking with 5 % BSA for 30 min. Following this, the sections were left to incubate overnight at 4 °C with the primary antibodies, including FBXO40 (Bioss, cat.number bs-16049R), TRIM63 (Proteintech, cat.number 55456-1-AP), PTX3 (Abcam, cat.number ab90806), and IGF2BP2 (Abcam, cat.number ab124930), before being exposed to HRP-labeled goat anti-rabbit IgG (H + L) (Beyotime, Shanghai, China, cat.number A0208). Color development was achieved by treating the sections with 3, 3′-

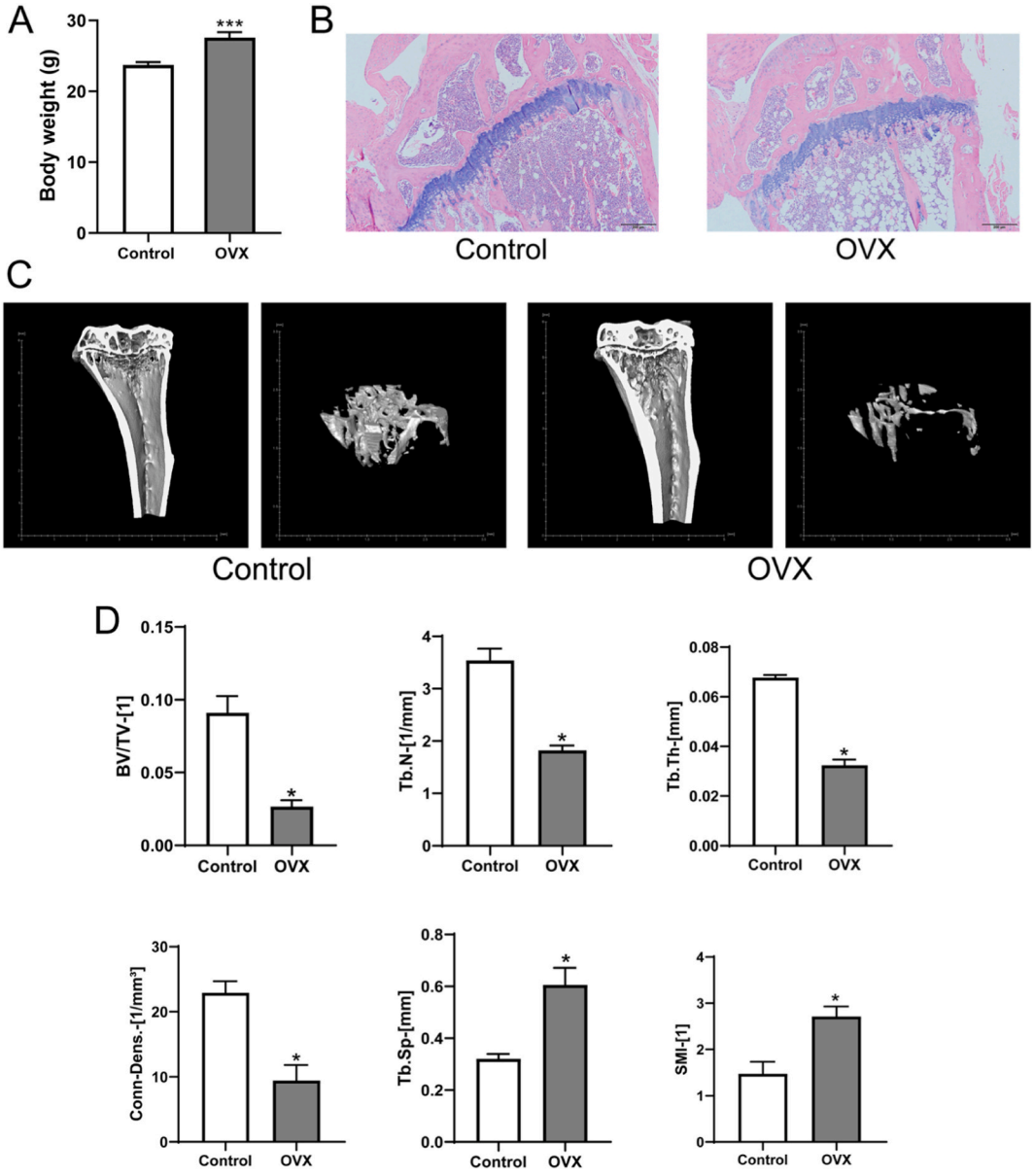

Fig. 1. Assessment of bone mass in mice. (A) Statistics on the body weights of mice at 12 weeks post-OVX (the OVX group) and sham operation (the control group). (B) Evaluation of pathological structural alterations in the proximal tibias of the control and OVX groups was performed using H&E staining, scale bar = 200 μm. (C) Micro-CT was employed to assess the bone microstructure in the proximal tibias of mice. (D) The parameters included BV/TV, Tb. N, Tb. Th, Conn. D, Tb. Sp, and SMI, $*p < 0.05$, n = 5.

diaminobenzidine, and then counterstaining them with hematoxylin. The treated slices were made transparent using xylene, dehydrated in ethanol, sealed with neutral gum, and photographed under an Olympus microscope.

2.10. Statistical analysis

SPSS software (IBM, New York, NY, USA) was utilized for data analysis. Descriptive statistics were employed to display the mean ± standard deviation (SD) of the data, and group differences were evaluated through one-way ANOVA. $p < 0.05$ indicated a significant difference.

3. Results

3.1. Bone mass was lost in ovariectomized mice

Among the 12-week-old female C57BL/6J mice selected, six underwent OVX, and the remaining control mice had adipose tissue

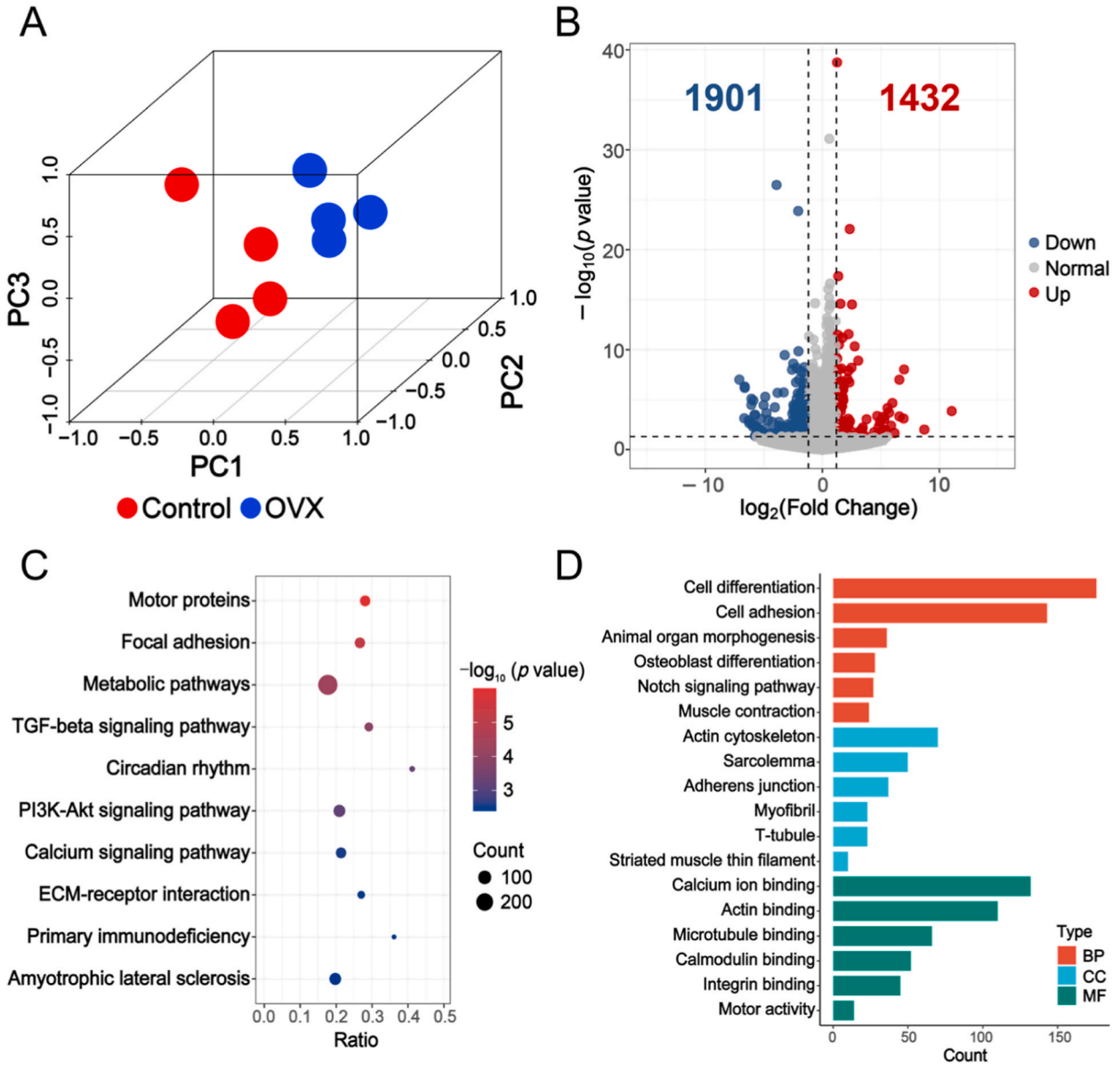

Fig. 2. (A) PCA for the mRNA expression between the OVX and control groups. (B) Volcano plot depicting genes expression, with down-regulated (in blue) or up-regulated (in red). The (C) GO and (D) KEGG enrichments of DEGs.

removal. After 12 weeks, the body weights of the mice were measured and bone mass evaluation was conducted to confirm the successful establishment of the OP model. As is presented in Fig. 1A, in comparison with the control group whose fat had been removed, the body weights of the ovariectomized mice increased. The bone tissue structure and cellular alterations in the tibias were assessed through H&E staining, revealing that ovariectomized mice exhibited deteriorated bone architecture characterized by reduced trabecular density and diminished bone marrow cellularity (Fig. 1B). The micro-CT evaluation of the tibias revealed significant damage to the cancellous bone in the OVX group (Fig. 1C). Moreover, the parameters exhibited a negative correlation with bone mass, including BV/TV, Tb. N, Tb. Th, and Conn. D, which were reduced. The negative correlation indices of Tb. Sp and SMI exhibited a significantly increase (Fig. 1D). The findings of this study demonstrated that OVX induced bone loss in mice.

3.2. DEGs annotations

Principal component analysis (PCA) revealed significant differences between the OVX group and control group based on the analysis of RNA-seq data (Fig. 2A). A total of 3333 genes were found to be differentially expressed, with 1901 down-regulated and 1432 up-regulated based on a screening criterion of $p < 0.05$ and fold change $\geq$1.2 when comparing the OVX group to the control group or vice versa (Fig. 2B). The DAVID database was utilized to perform KEGG and GO enrichment analyses on DEGs. The KEGG pathways included focal adhesion, TGF-beta signaling pathway, and amyotrophic lateral sclerosis (Fig. 2C), while the GO terms included animal organ morphogenesis, sarcolemma, and muscle contraction (Fig. 2D). GSEA analysis of the OVX group revealed significant inhibition in muscle contraction, sarcolemma, animal organ morphogenesis, and TGF-beta signaling pathway compared to the control group (Fig. 3).

3.3. m6A modification pattern in ovariectomized mice

After conducting MeRIP-seq analysis, a total of 64,613 m6A peaks corresponding to 14,600 m6A genes have been identified in the

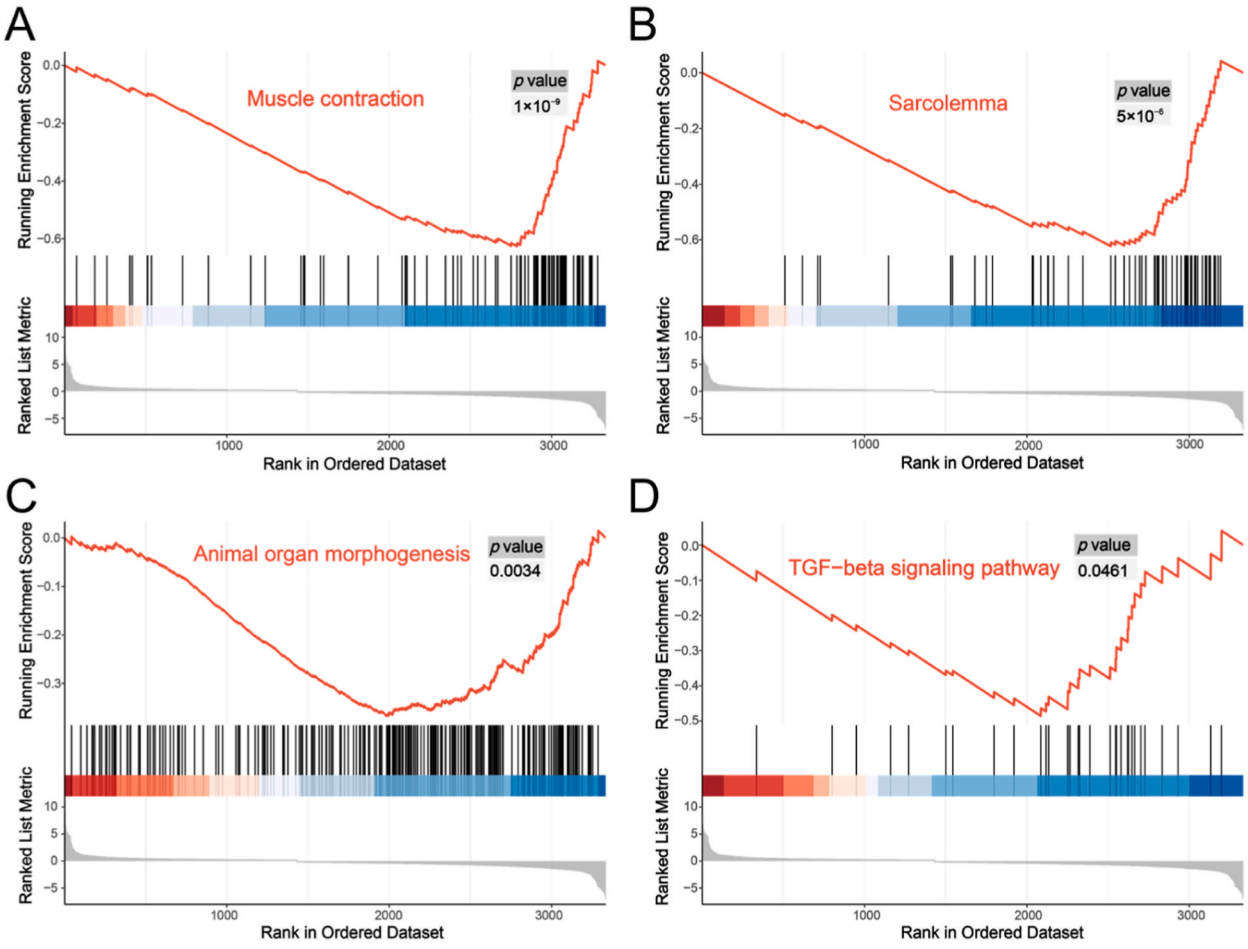

Fig. 3. GSEA revealed that genes were enriched for (A) muscle contraction, (B) sarcolemma, (C) animal organ morphogenesis, and (D) TGF-beta signaling pathway in OVX group.

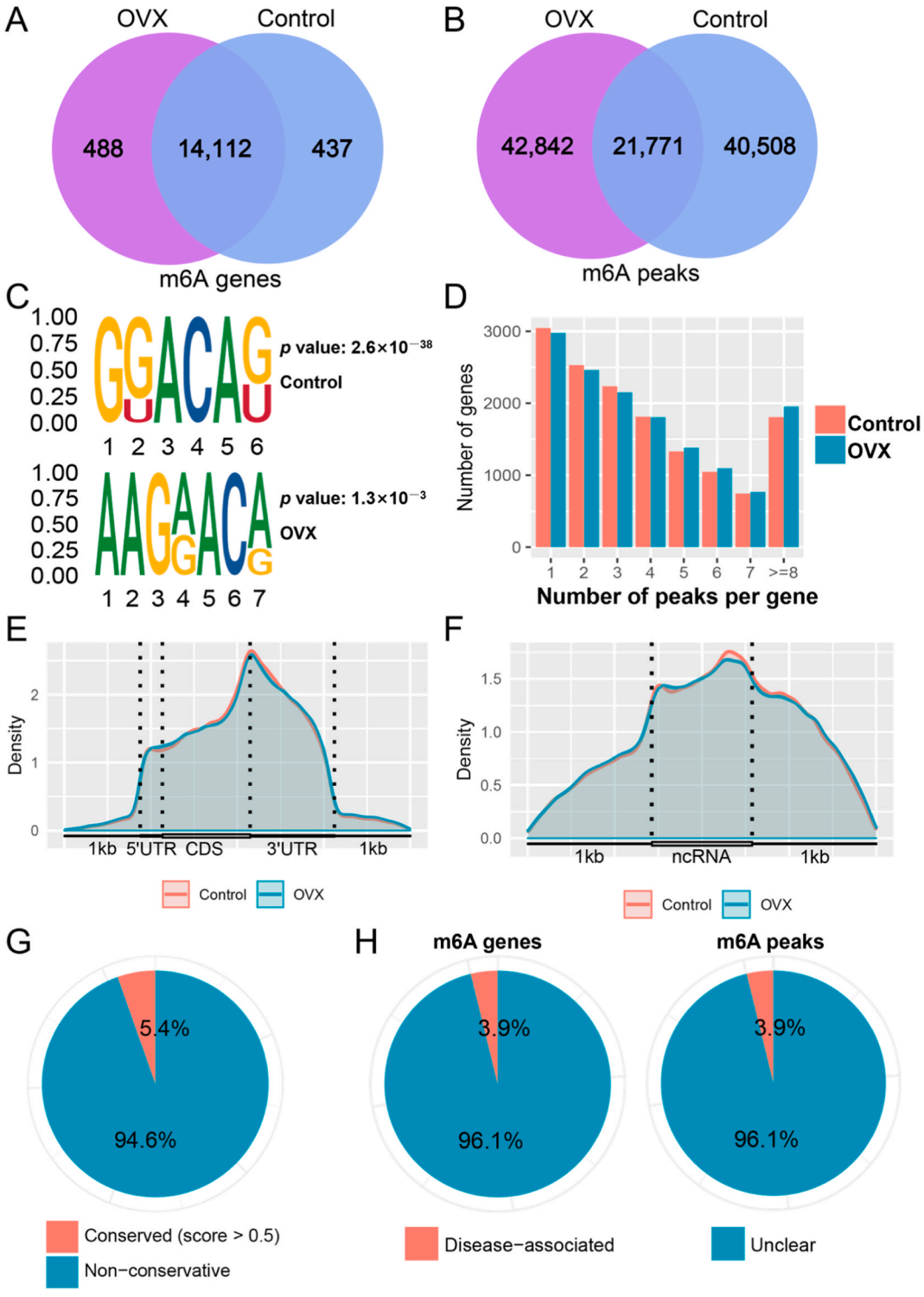

Fig. 4. Patterns of m6A modifications in the OVX group and the control group. Venn diagrams showing overlap of (A) m6A genes and (B) m6A peaks between both groups. (C) Motifs enriched from identified m6A peaks. (D) Quantitative distribution of m6A-modified peaks per gene. Distribution of m6A peaks in the (E) mRNAs and (F) ncRNAs. (G) Conserved and non-conserved m6A sites. (H) The disease association of m6A genes and m6A peaks.

OVX group. Similarly, in the control group, 62,279 m6A peaks were detected, corresponding to 14,549 m6A genes. Furthermore, 21,771 peaks corresponding to 14,112 genes were identified in the overlapping regions between the OVX and control groups (Fig. 4A and B). The RRACH sequence has been identified as the consensus sequence of m6A modification in the nucleotranscriptome of mammals, where R represents A/G, H corresponds to A/C/U, and A denotes m6A. We employed STREME to delineate the conserved RRACH sequence, and our findings revealed the presence of this sequence in both groups (Fig. 4C). Subsequently, the quantification of m6A-methylated transcripts was performed to ascertain the quantitative distribution of m6A peaks per gene, revealing that a majority of genes exhibited 1–4 peaks (Fig. 4D).

Analysis was carried out on the distribution patterns of m6A peaks in mRNAs and ncRNAs between the OVX and control groups. The results indicated no significant variances in the distribution patterns between the two groups. In m6A-modified mRNAs, the m6A peaks were mostly concentrated in the coding sequence (CDS) and 3′ untranslated region (3′UTR). Notably, the highest density of m6A peaks was observed proximal to the stop codon segment (Fig. 4E). In the ncRNAs, the density of m6A peaks increased relatively gently and displayed an even distribution throughout the sequence (Fig. 4F). Through the analysis of differentially modified m6A and DEGs, it was revealed that only 5.4 % of the m6A-modified sites exhibited conservation (Fig. 4G), while 3.9 % of both the m6A genes and m6A peaks were associated with disease (Fig. 4H).

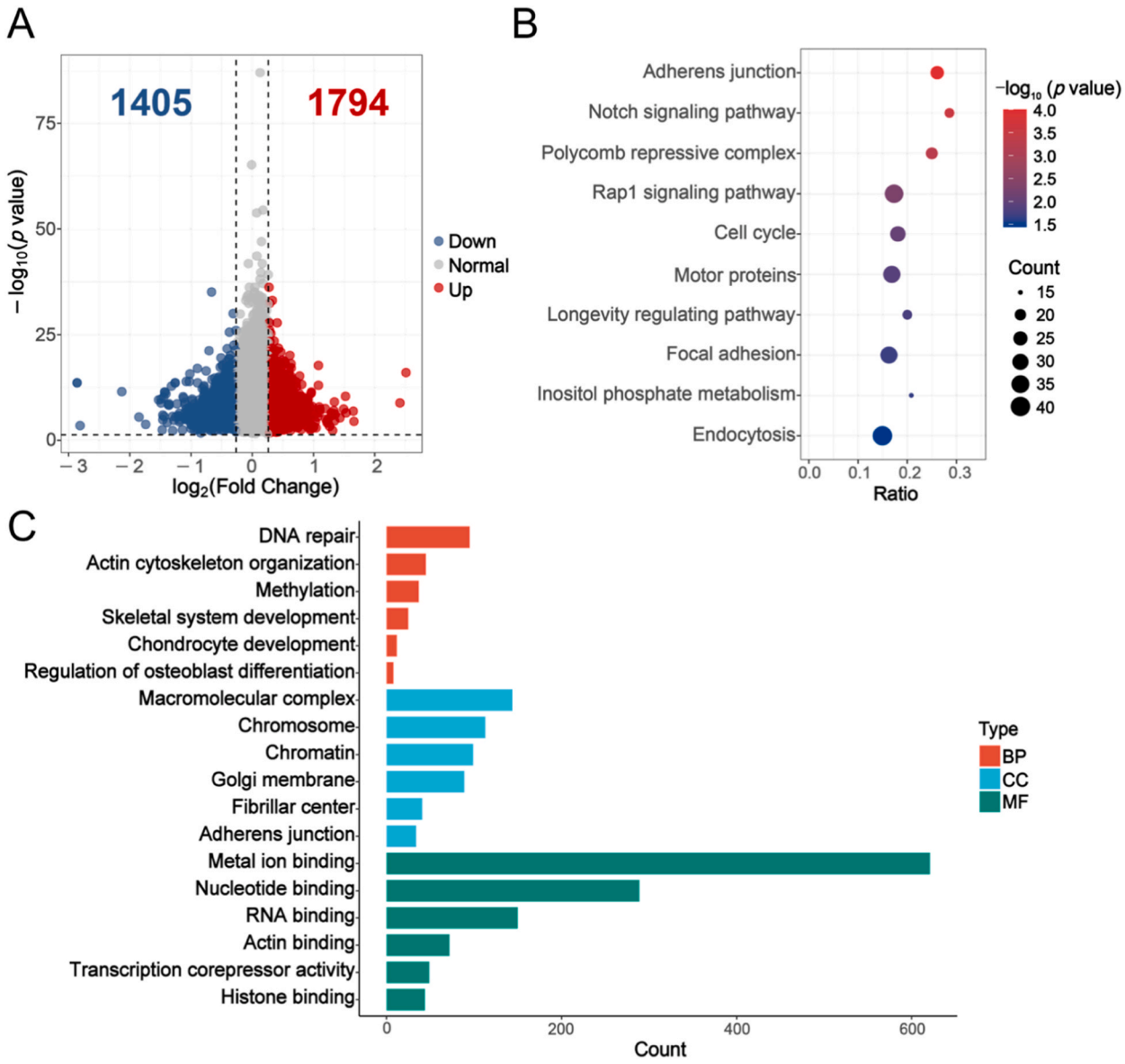

Fig. 5. (A) Volcano plot of m6A modification sites, with down-regulated (in blue) or up-regulated (in red). The (B) GO and (C) KEGG enrichments of differentially m6A-modified mRNAs.

3.4. The annotations of differentially m6A-modified mRNAs

By analyzing the m6A-seq data using a statistical threshold of $p < 0.05$ and fold change ≥ 1.2 when comparing the OVX group to the control group or vice versa, we discovered 2586 mRNAs with 3199 differentially m6A modification sites between the OVX group and the control group (Fig. 5A). Enrichment analyses were conducted on the 2586 mRNAs, revealing terms such as Notch signaling pathway, Rap1 signaling pathway, motor proteins for KEGG (Fig. 5B), and skeletal system development, regulation of osteoblast differentiation, metal ion binding for GO (Fig. 5C).

3.5. The annotations for genes with differential methylation and expression

By analyzing the RNA-seq data and the m6A-seq data, an overlap of 582 genes between 2586 differentially m6A-modified mRNAs and 3333 DEGs were observed (Fig. 6A). Enrichment analysis was conducted on these overlapping genes using GO and KEGG. The results of the KEGG pathway analysis indicated the involvemen of overlapping genes in critical signaling pathways, including Notch signaling, TGF-beta signaling, Rap1 signaling, and cell adhesion molecules et al. (Fig. 6B). The GO enrichment analysis was categorized into BP, CC, and MF. The BP terms encompassed aging, positive regulation of osteoblast differentiation, and skeletal system morphogenesis. Regarding CC, the terms centered around calcium channel complex and sarcolemma. Lastly, the MF terms included metal ion binding (Fig. 6C).

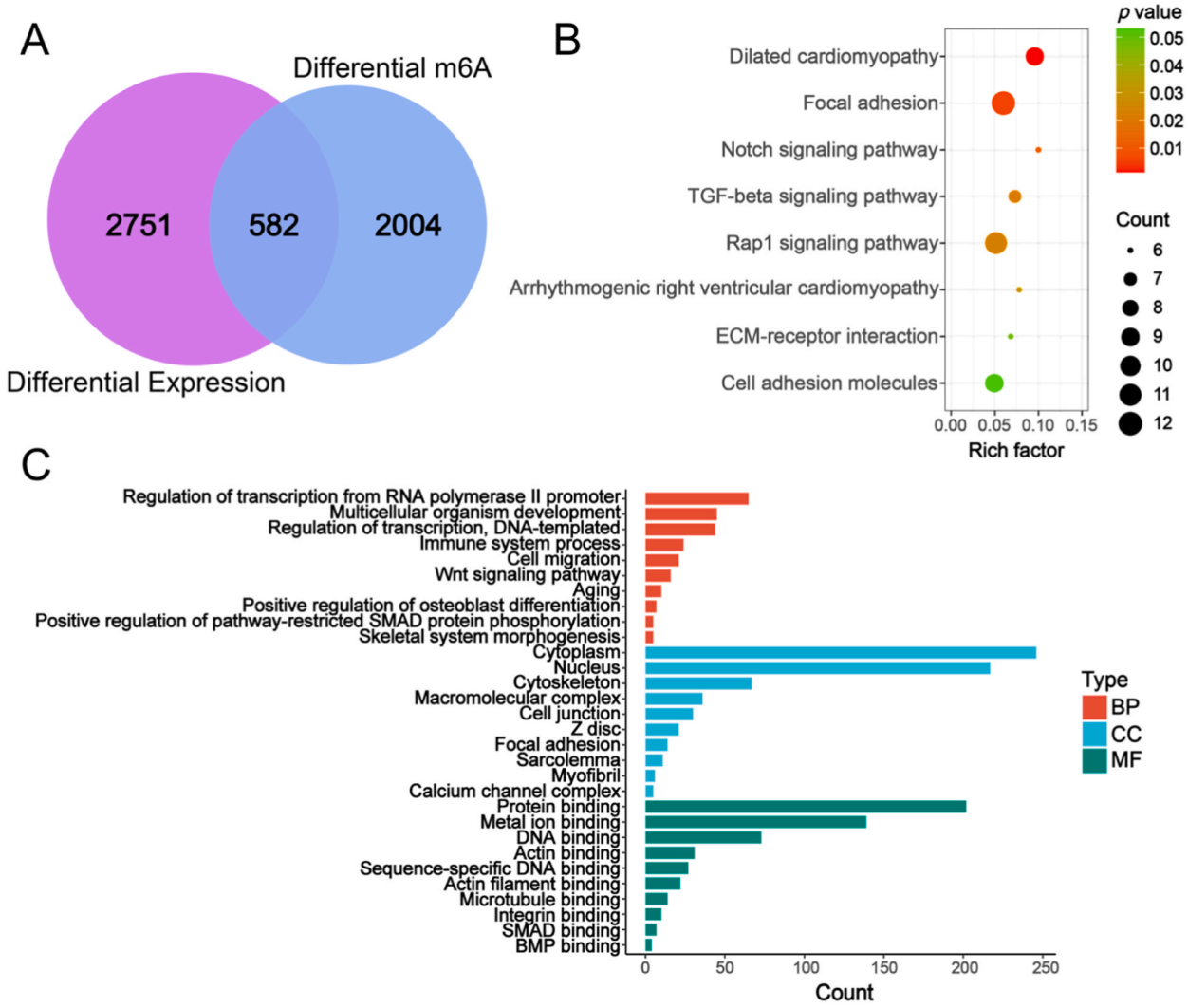

Fig. 6. (A) DEGs and differential m6A-modified mRNAs between the OVX and control groups. (B) KEGG analysis enriched pathways and (C) GO functional annotation of the 582 overlapping DEGs.

3.6. Potential regulators and their substrates

To explore the patterns of m6A modification, an analysis was conducted on the mRNA expression levels of RNA m6A regulators in this study, resulting in the identification of potential regulators involved in RNA m6A methylation. Significant expression differences ($p < 0.05$) were observed among three writers, three readers, and one eraser, as presented in Table 1. Among them, the expression levels of *Rbm15b*, *Rbm15* and *Mettl3* as writers were up-regulated, while the readers *Ythdf2* and *Igf2bp3* were also up-regulated. Conversely, down-regulation of the reader *Igf2bp2* and the eraser *Fto* was observed.

According to the RNA-seq data, significant differences were observed in the mRNA expression levels of genes correlated with KEGG and GO terms related to bone formation and metabolism, which included Notch signaling pathway (*Dll4*, *Rbpj*, *Tle3*, *Dtx1*, *Notch3*), TGF-beta signaling pathway (*Zfyve9*, *Bmpr2*, *Smurf1*, *Bmp5*, *Tgfb3*), Rap1 signaling pathway (*Crkl*, *Efna1*, *Tln2*, *Plce1*, *Pdgfra*), cell adhesion molecules (*Itga8*, *Cd34*, *Sdc1*, *Itga4*, *Cdh5*) and metal ion binding (*Rag2*, *Zbtb7a*, *Pdzrn3*, *Fbxo40*, *Trim63*) as shown in Table 2.

We subsequently established a PPI network to investigate the regulatory relationship between genes associated with the aforementioned key terms and 7 differentially expressed regulators (Fig. 7A). The regulators IGF2BP2, IGF2BP3, RBM15B, FTO, YTHDF2, METTL3 and RBM15 exhibited degrees of 4, 4, 6, 6, 7, 7 and 8, respectively. The levels of m6A methylation on the mRNA transcript were observed, as indicated by the IGV displays (Fig. 7B). It is notable that the genes associated with bone formation and metabolism demonstrated a reduced level of m6A methylation in the OVX group. GSEA analysis of the OVX group revealed significant inhibition in skeletal system morphogenesis, cell junction, and actin binding compared to the control group (Fig. 8A, B and C). The heatmap depicting DEGs enriched in the key terms related to bone formation and metabolism was generated to validate the expression disparities between the control and OVX groups (Fig. 8D).

3.7. Variant landscape of the control and ovariectomized mice

We have carried out an analysis of the mutation status of genes in control and ovariectomized mice, among which nonsynonymous single nucleotide variants (SNV) were the most common type of mutations (Fig. 9A and B), SNPs showed a much higher proportion in the type of variation than insertions (INS) and deletions (DEL) (Fig. 9C), and T > C was the most common SNV class (Fig. 9E and F). In addition, the top 10 mutated genes in ovariectomized mice were also presented (Fig. 9D).

3.8. Validation of significant m6A regulators and potential hub genes

Protein-level expression patterns of potential regulators and biomarkers related to bone metabolism were investigated using the western blotting assay. The expression levels of FBXO40, TRIM63, PTX3, and IGF2BP2 were found to be reduced in the OVX group (Fig. 10A), and the original images for the three replicates were presented in Fig. S1. The immunohistochemical staining results were consistent with those obtained from western blotting, revealing weak expression of FBXO40, TRIM63, PTX3, and IGF2BP2 in the OVX groups (Fig. 10B). Therefore, these findings suggested a crucial involvement of m6A regulators in bone metabolism.

Table 1
The mRNA expression levels of m6A regulators.

Gene	Regulation	Base Mean	Log_2FoldChange	*p* value
Rbm15b	writer	2932.51	0.3375	4.09×10^{-9}
Rbm15	writer	1834.35	0.5058	1.83×10^{-8}
Igf2bp2	reader	197.40	−0.5801	2.15×10^{-3}
Ythdf2	reader	1852.65	0.2303	3.55×10^{-3}
Mettl3	writer	1352.54	0.3166	4.87×10^{-3}
Fto	eraser	2966.70	−0.1810	1.36×10^{-2}
Igf2bp3	reader	49.12	0.8366	3.75×10^{-2}
Cbll1	writer	366.63	0.2504	7.24×10^{-2}
Mettl5	writer	491.81	−0.1291	1.42×10^{-1}
Hnrnpa2b1	reader	61893.59	0.1546	1.49×10^{-1}
Ythdf3	reader	2588.89	0.1511	2.09×10^{-1}
Ythdf1	reader	1600.10	0.0884	3.31×10^{-1}
Hnrnpc	reader	15752.64	0.1393	3.52×10^{-1}
Alkbh5	eraser	5102.10	−0.1027	4.69×10^{-1}
Ythdc2	reader	1540.22	0.0582	4.90×10^{-1}
Virma	writer	5471.03	0.0512	5.92×10^{-1}
Zc3h13	writer	11094.88	0.0318	6.33×10^{-1}
Ythdc1	reader	13115.91	−0.0372	7.30×10^{-1}
Wtap	writer	4185.47	0.0303	7.59×10^{-1}
Mettl14	writer	2334.99	−0.0108	9.07×10^{-1}
Fmr1	reader	5716.39	−0.0032	9.76×10^{-1}
Igf2bp1	reader	1.1128	0.0942	9.78×10^{-1}

Table 2
The mRNA expression levels of potential substrates and regulators.

	Gene	$\log_2$ Fold Change	*p* adj	Reader			Writer	Eraser
				YTHDF2	IGF2BP3	IGF2BP2	METTL3	FTO
Notch signaling pathway	*Dll4*	−0.7753	1.78×10^{-2}	N	Y	Y	N	N
	Rbpj	−0.2678	3.26×10^{-2}	N	N	Y	N	Y
	Tle3	0.2879	1.12×10^{-1}	N	N	Y	Y	Y
	Dtx1	0.5646	1.40×10^{-1}	N	N	Y	N	Y
	Notch3	−0.4732	1.59×10^{-1}	Y	Y	Y	N	Y
TGF-beta signaling pathway	*Zfyve9*	−0.8374	6.69×10^{-3}	N	Y	Y	N	Y
	Bmpr2	−0.4609	6.26×10^{-2}	N	Y	Y	Y	Y
	Smurf1	−0.3066	1.30×10^{-1}	Y	N	Y	Y	Y
	Bmp5	−0.5739	1.42×10^{-1}	N	Y	Y	N	Y
	Tgfb3	−0.5448	1.62×10^{-1}	N	N	Y	N	Y
Rap1 signaling pathway	*Crkl*	0.3221	4.30×10^{-3}	Y	N	Y	Y	Y
	Efna1	−0.7176	4.31×10^{-3}	N	Y	N	N	N
	Tln2	−0.7113	7.00×10^{-2}	N	Y	Y	N	Y
	Plce1	−0.7591	1.29×10^{-1}	N	N	Y	N	Y
	Pdgfra	−0.5744	1.91×10^{-1}	N	N	Y	N	Y
Cell adhesion molecules	*Itga8*	−1.2474	1.09×10^{-3}	N	Y	Y	N	Y
	Cd34	−0.3598	8.49×10^{-3}	N	Y	Y	N	N
	Sdc1	−0.3515	2.01×10^{-2}	N	Y	Y	N	N
	Itga4	0.2891	7.51×10^{-2}	N	N	Y	N	Y
	Cdh5	−0.4774	1.60×10^{-1}	N	Y	Y	N	Y
metal ion binding	*Rag2*	2.7645	1.89×10^{-8}	N	Y	N	N	N
	Zbtb7a	0.3050	1.45×10^{-7}	N	N	Y	N	Y
	Pdzrn3	−1.5288	1.23×10^{-4}	N	N	Y	N	Y
	Fbxo40	−1.9272	7.76×10^{-4}	N	Y	N	Y	Y
	Trim63	−2.4791	1.31×10^{-3}	N	N	N	N	N

Y represents the mRNA is the substrate of the RNA m6A regulators, and N represents not.

4. Discussion

OP is currently recognized as the most prevalent bone disorder worldwide, characterized by a progressive decline in bone mass, particularly among elderly females [31]. Disruptions in bone homeostasis caused by abnormal bone metabolism can give rise to OP and other bone-related disorders [32]. Epigenetic modifications include DNA, RNA and histone modifications, which can regulate gene expression and translation [33]. A study has found that the regulation of gene expression through DNA methylation sites may contribute to the development of knee osteoarthritis [34]. In addition, other studies have also revealed that m6A methylation is implicated in the progression of bone-related, such as osteoporosis, osteoarthritis, and osteosarcoma [35], suggesting a fundamental basis for understanding the impact of m6A modification on OP and its potential implications for preventive and therapeutic interventions.

Analysis of the sequencing data from the OVX group and the control group revealed a common motif sequence, RRACH [36]. Additionally, as previously reported, most m6A modification transcripts exhibited a significant enrichment in the CDS region, with the highest level observed proximal to the stop codon [37]. The increased abundance of m6A modification sites located at the stop codon could potentially influence mRNA stability, translation, and decay processes [38]. After undergoing OVX, enrichment analyses of GO terms and KEGG pathways were performed for the 582 DEGs with differentially m6A modification to assess the alterations in biological functions caused by RNA m6A modification. We found that most of the enriched terms were related to bone formation and metabolism. The modulation of Notch signaling pathway exerts an impact on the lineage commitment of mesenchymal stem cells towards osteocytes, thereby playing a critical role in maintaining the homeostasis between osteoblasts and osteoclasts [39]. TGF-β is the most abundant cytokine in bone tissue [40], where it exerts its effects by promoting osteoblast proliferation and differentiation, as well as regulating bone remodeling processes to maintain optimal bone metabolism balance [41]. Rap1, a small GTPase, is involved in MAPK signaling pathway which has been demonstrated to be of significant importance in both osteoblast and osteoclast biology [42]. Moreover, cell adhesion molecules are involved in controlling the differentiation and formation of osteocytes [43], and metal ion binding plays a significant role in promoting bone tissue growth.

The regulation of mRNA m6A methylation involves methyltransferases, methylation binding proteins, and demethylasess, while the existing m6A research on bones mainly focuses on writers [35]. In this study, we revealed a significant decrease in the expression levels of FBXO40, TRIM63, PTX3, and IGF2BP2 in the OVX group compared to the control group. IGF2BP2, as a reader, was found that its depletion decelerated osteoblast proliferation while promoting osteogenic differentiation, and the expression of IGF2BP2 is influenced by the occurrence of OP [44]. The expression of FBXO40, which is specific to muscle tissue, exhibits a decline concomitant with the reduction in muscle cell differentiation [45]. An examination of muscle condition and OP in 313 women with hip fractures has observed that OP is associated with loss of skeletal muscle mass, as sarcopenia was found in 58 % of the participants and OP in 74 % [46]. Consequently, the expression of FBXO40 may be diminished in individuals with OP. Previous studies have elucidated that TRIM63, an E3 ubiquitin ligase primarily expressed in muscle tissue, exerts inhibitory effects on proliferation and promotes differentiation of osteoblastic cells [47]. Moreover, PTX3 maintains bone homeostasis *in vivo* by coordinating the biological functions of

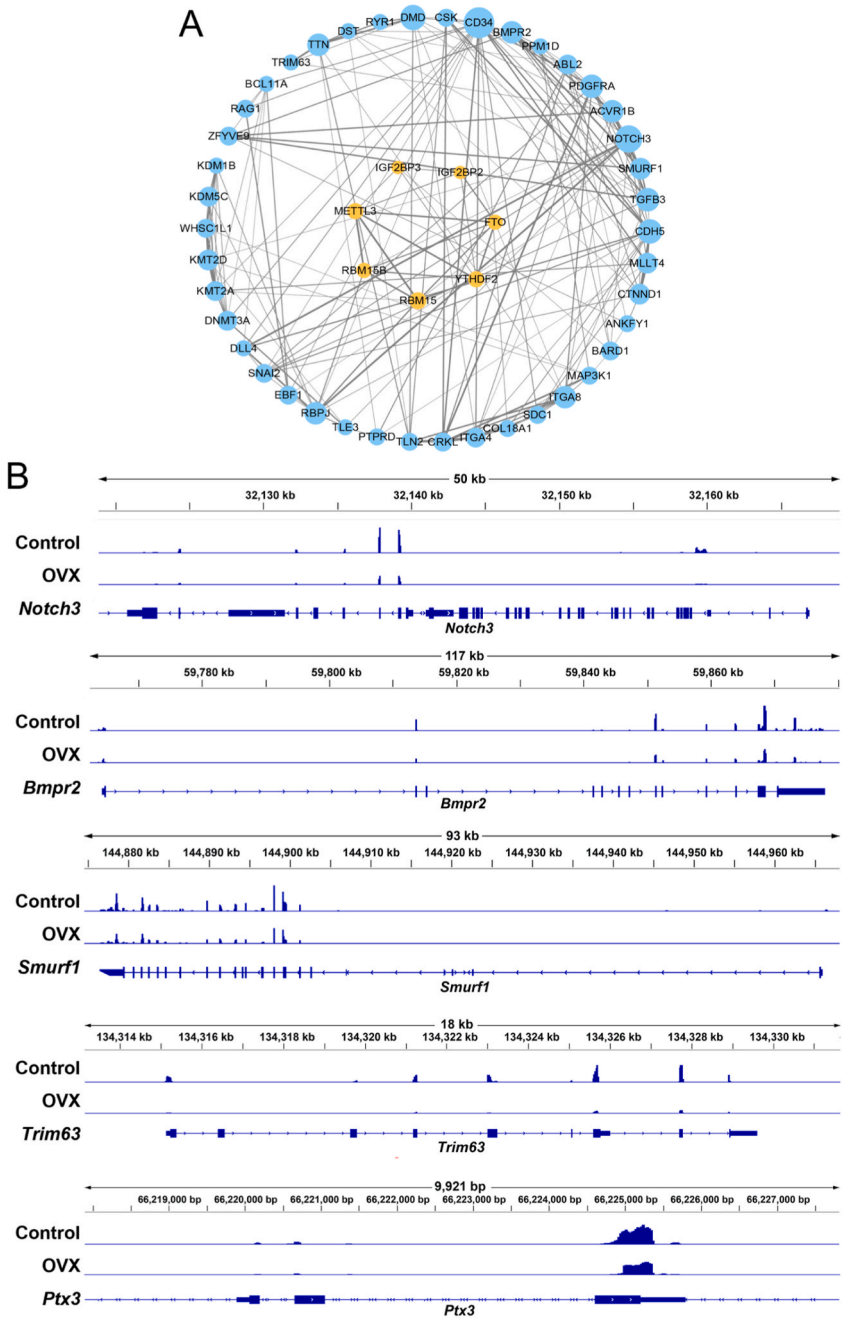

Fig. 7. (A) The PPI built with m6A regulators (yellow circle) and genes (blue circle) from KEGG and GO terms related to bone formation and metabolism. (B) The level of m6A on *Notch3*, *Bmpr2*, *Smurf1*, *Trim63*, and *Ptx3* mRNA transcripts observed by IGV.

osteoblasts and osteoclasts, while simultaneously regulating the equilibrium between bone formation and resorption [48]. Therefore, in combination with the research findings, it is indicated that these proteins and the reader IGF2BP2 played crucial roles in the occurrence and development of osteoporosis.

Furthermore, we analyzed the variant landscape of ovariectomized mice, the top 3 genes with the highest number of mutations were *Ttn*, *Obscn*, and *Syne2*. Titin encoded by *Ttn* is the largest known protein, widely expressed in skeletal muscles, and pathogenic variations in *Ttn* can cause a series of skeletal phenotypes [49,50]. *Obscn*, the gene for obscurin, can be expressed in locations such as the femur and humerus, cortical bone, and tendons [51]. *Syne2* encodes Nesprin-2, which belongs to the nuclear envelope spectrin repeat protein family, and variations in *Syne2* are associated with autosomal dominant Emery Dreifuss muscular dystrophy 5 [52]. The variations in these genes may be associated with the occurrence of osteoporosis, while the impact of genomic variations after OVX on

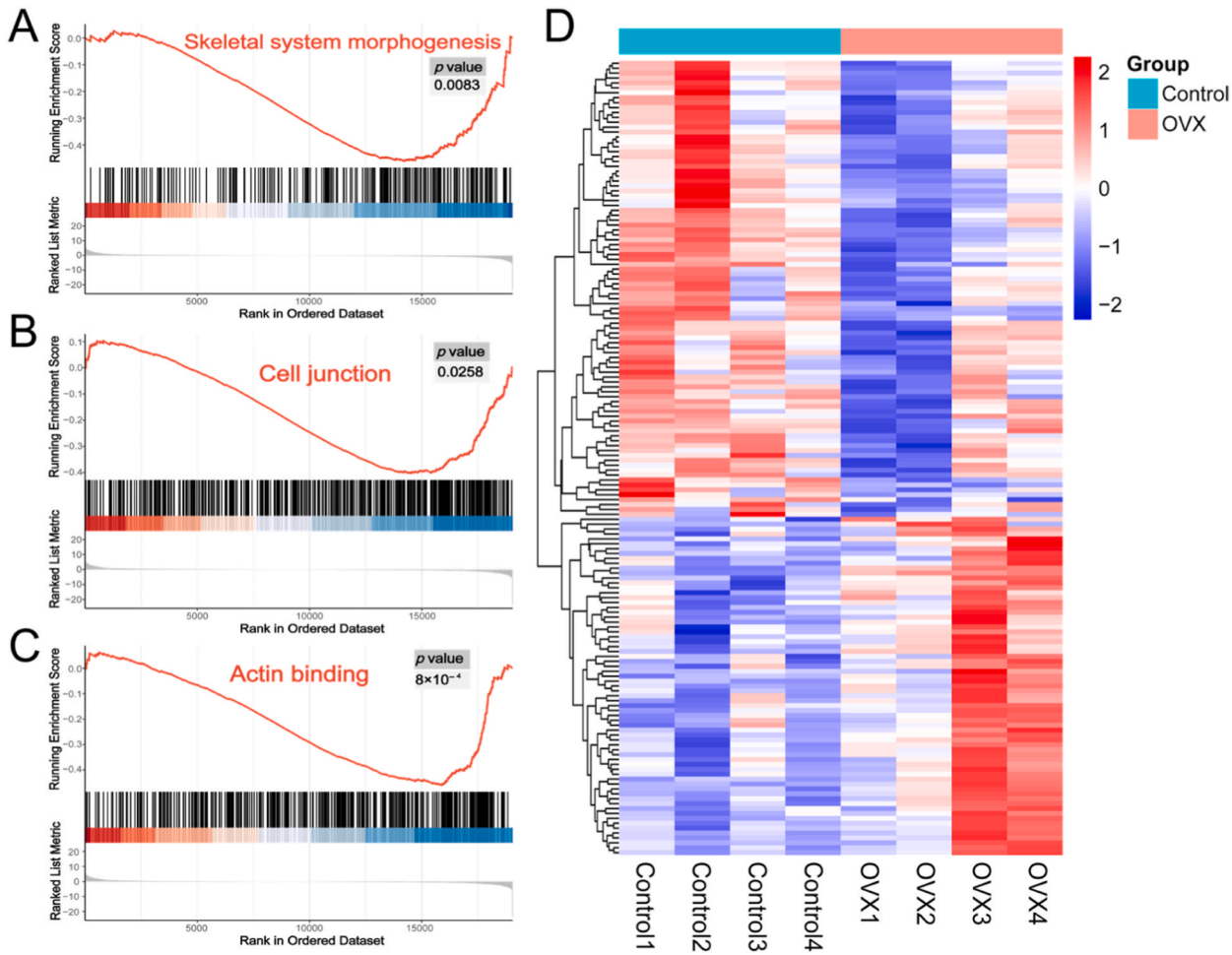

Fig. 8. GSEA of the (A) skeletal system morphogenesis, (B) cell junction and (C) actin binding in the OVX group compared with the control group. (D) Heatmap of parts of DEGs in the OVX and control groups.

osteoporosis remains to be further investigated.

Our findings have provided confirmation that m6A methylation is involved in the regulation of bone metabolism, thereby shedding novel insights into the involvement of m6A regulators in the pathogenesis of OP, which further illustrated the potential significance of m6A regulators in OP development. However, there are several limitations in our study. Firstly, the differentially expressed gene profile was generated from mice models due to ethical and social governance constraints, which may limit the credibility of our findings compared to human samples. Additionally, the regulatory mechanisms underlying m6A modification in bone metabolism during OP progression remain incompletely understood, including the coordination between writers and erasers, as well as the function of readers upon RNA methylation recognition. Therefore, we will continue to explore and verify these issues.

5. Conclusion

In summary, we have presented preliminary findings on gene expression changes and explored the involvement of m6A regulators in OP by examining m6A modification patterns and expression profiles in ovariectomized mice. The disturbance of m6A methylation levels in target genes and the aberrant expression of m6A regulators impacted mRNA stability, translation, and decay processes. Overall, our results suggested that m6A modification significantly contributed to the pathogenesis of OP, providing valuable insights for further elucidating the mechanisms underlying m6A regulators in OP.

CRediT authorship contribution statement

Lifeng Zheng: Writing – original draft, Investigation, Funding acquisition, Formal analysis, Conceptualization. **Chao Lan:** Writing – original draft, Investigation, Formal analysis. **Xinyue Gao:** Writing – original draft, Investigation, Formal analysis. **An Zhu:** Investigation, Data curation. **Yaoqing Chen:** Investigation, Data curation. **Jinluan Lin:** Investigation, Data curation. **Sunjie Yan:**

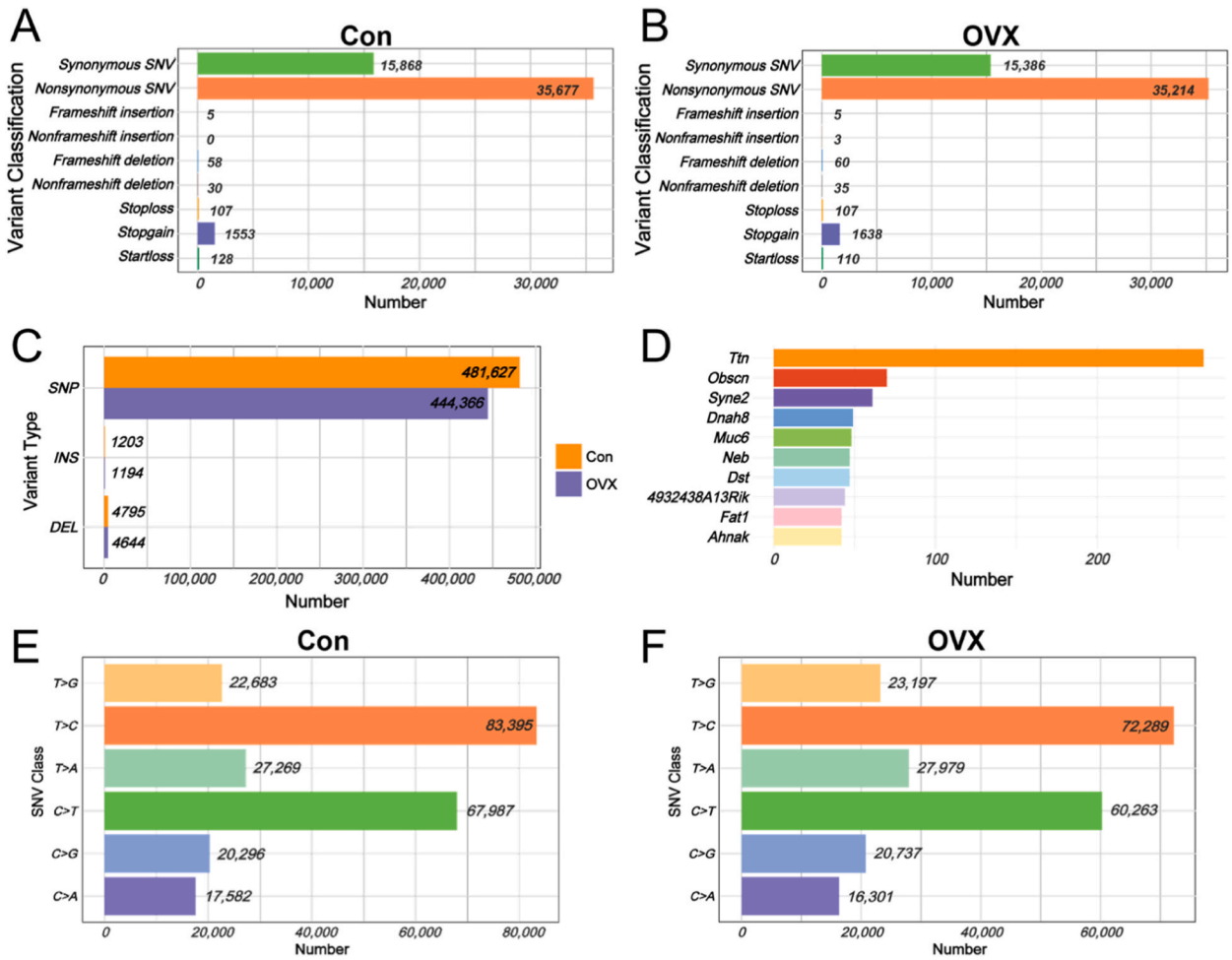

Fig. 9. An overview of mutation information in the control and OVX groups. Classification and statistics of variants in (A) the control group and (B) the OVX group. (C) Statistics of variant types. (D) The top 10 genes with the highest number of mutations in the OVX group. Subdivision statistics of SNV class in (E) the control group and (F) the OVX group.

Investigation. **Ximei Shen:** Writing – review & editing, Funding acquisition.

Data availability statement

Data associated with study have deposited into a publicly available repository. MeRIP data have been deposited at datatype-specific repository (https://www.ncbi.nlm.nih.gov/geo/) with accession numbers GSE277491.

Ethics approval

This study was approved by the Experimental Animal Ethical Committee of Fujian Medical University with the number of IACUC FJMU 2022-NSFC-0201.

Funding

This research was funded by the Fujian Provincial Health Technology Project (2022GGA024), the Leading Project Foundation of Science and Technology, Fujian Province (2023Y0016), the Scientific and Technological Innovation of Fujian Province Project (2021Y9109), and the Fujian Province Finance Project (BPB-2021ZLF).

Declaration of competing interest

The authors declare that they have no known competing financial interests or personal relationships that could have appeared to

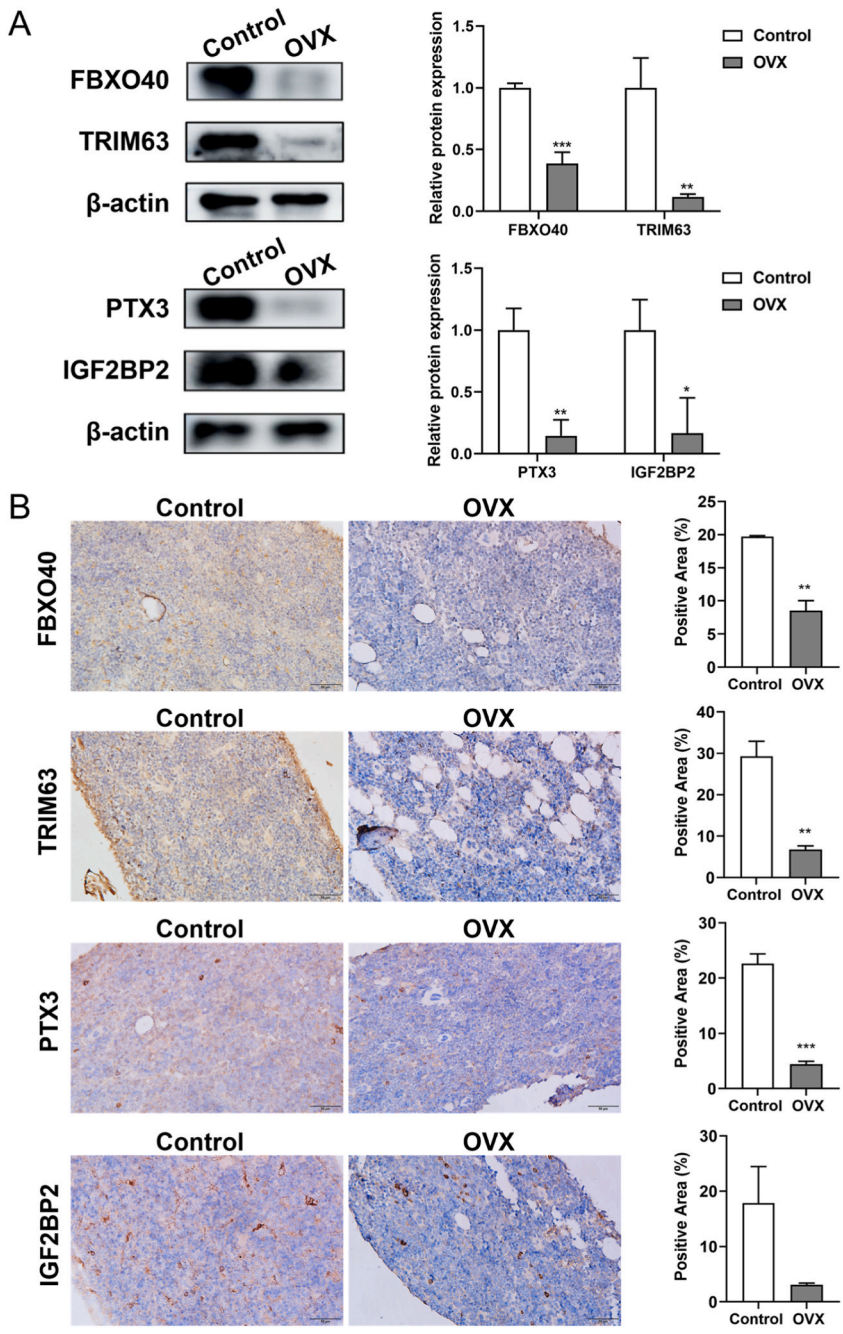

Fig. 10. (A) Western blotting of FBXO40, TRIM63, PTX3, and IGF2BP2 in the control and OVX groups. (B) Immunohistochemical staining of FBXO40, TRIM63, PTX3 and IGF2BP2 protein expression in the tibial sections with different treatments, scale bar = 50 μm, $*p < 0.05$, $**p < 0.01$, and $***p < 0.001$, n = 3.

influence the work reported in this paper.

Appendix A. Supplementary data

Supplementary data to this article can be found online at https://doi.org/10.1016/j.heliyon.2025.e42123.

References

[1] P.D. Miller, Management of severe osteoporosis, Expet Opin. Pharmacother. 17 (2016) 473–488.
[2] P.D. Delmas, Treatment of postmenopausal osteoporosis, Lancet 359 (2002) 2018–2026.
[3] J.Y. Reginster, N. Burlet, Osteoporosis: a still increasing prevalence, Bone 38 (2006) S4–S9.
[4] J.A. Kanis, E.V. McCloskey, H. Johansson, et al., European guidance for the diagnosis and management of osteoporosis in postmenopausal women, Osteoporos. Int. 24 (2013) 23–57.
[5] K.G. Cotts, A.S. Cifu, Treatment of osteoporosis, JAMA 319 (2018) 1040–1041.
[6] E. Bonucci, P. Ballanti, Osteoporosis-bone remodeling and animal models, Toxicol. Pathol. 42 (2014) 957–969.
[7] Y. Chen, Z. Xie, Y. Zhang, et al., Shikonin relieves osteoporosis of ovariectomized mice by inhibiting RANKL-induced NF-κB and NFAT pathways, Exp. Cell Res. 394 (2020) 112115.
[8] L. Yin, X. Zhu, P. Novák, et al., The epitranscriptome of long noncoding RNAs in metabolic diseases, Clin. Chim. Acta 515 (2021) 80–89.
[9] W. Wei, X. Ji, X. Guo, et al., Regulatory role of N(6) -methyladenosine (m(6) A) methylation in RNA processing and human diseases, J. Cell. Biochem. 118 (2017) 2534–2543.
[10] S. Panneerdoss, V.K. Eedunuri, P. Yadav, et al., Cross-talk among writers, readers, and erasers of m(6)A regulates cancer growth and progression, Sci. Adv. 4 (2018) eaar8263.
[11] Y. Wu, C. Zhou, Q. Yuan, Role of DNA and RNA N6-adenine methylation in regulating stem cell fate, Curr. Stem Cell Res. Ther. 13 (2018) 31–38.
[12] W. Zhao, X. Qi, L. Liu, et al., Epigenetic regulation of m(6)A modifications in human cancer, Mol. Ther. Nucleic Acids 19 (2020) 405–412.
[13] S. Chen, Y. Li, S. Zhi, et al., WTAP promotes osteosarcoma tumorigenesis by repressing HMBOX1 expression in an m(6)A-dependent manner, Cell Death Dis. 11 (2020) 659.
[14] Y. Li, F. Yang, M. Gao, et al., miR-149-3p Regulates the switch between adipogenic and osteogenic differentiation of BMSCs by targeting FTO, Mol. Ther. Nucleic Acids 17 (2019) 590–600.
[15] Y. Wu, L. Xie, M. Wang, et al., Mettl3-mediated m(6)A RNA methylation regulates the fate of bone marrow mesenchymal stem cells and osteoporosis, Nat. Commun. 9 (2018) 4772.
[16] D. Li, L. Cai, R. Meng, et al., METTL3 modulates osteoclast differentiation and function by controlling RNA stability and nuclear export, Int. J. Mol. Sci. 21 (2020) 1660.
[17] R. Yu, Q. Li, Z. Feng, et al., m6A reader YTHDF2 regulates LPS-induced inflammatory response, Int. J. Mol. Sci. 20 (2019) 1323.
[18] C.J. Deselm, W. Zou, S.L. Teitelbaum, Halofuginone prevents estrogen-deficient osteoporosis in mice, J. Cell. Biochem. 113 (2012) 3086–3092.
[19] D. Kim, J.M. Paggi, C. Park, et al., Graph-based genome alignment and genotyping with HISAT2 and HISAT-genotype, Nat. Biotechnol. 37 (2019) 907–915.
[20] M. Pertea, D. Kim, G.M. Pertea, et al., Transcript-level expression analysis of RNA-seq experiments with HISAT, StringTie and Ballgown, Nat. Protoc. 11 (2016) 1650–1667.
[21] M.I. Love, W. Huber, S. Anders, Moderated estimation of fold change and dispersion for RNA-seq data with DESeq2, Genome Biol. 15 (2014) 550.
[22] Y. Tang, K. Chen, B. Song, et al., m6A-Atlas: a comprehensive knowledgebase for unraveling the N6-methyladenosine (m6A) epitranscriptome, Nucleic Acids Res. 49 (2021). D134-d43.
[23] T.L. Bailey, STREME: accurate and versatile sequence motif discovery, Bioinformatics 37 (2021) 2834–2840.
[24] Y. Wang, K. Chen, Z. Wei, et al., MetaTX: Deciphering the distribution of mRNA-related features in the presence of isoform ambiguity, with applications in epitranscriptome analysis, Bioinformatics 37 (2021) 1285–1291.
[25] X. Jiao, B.T. Sherman, W. Huang da, et al., DAVID-WS: a stateful web service to facilitate gene/protein list analysis, Bioinformatics 28 (2012) 1805–1806.
[26] B. Song, K. Chen, Y. Tang, et al., ConsRM: collection and large-scale prediction of the evolutionarily conserved RNA methylation sites, with implications for the functional epitranscriptome, Briefings Bioinf. 22 (2021) bbab088.
[27] K. Chen, B. Song, Y. Tang, et al., RMDisease: a database of genetic variants that affect RNA modifications, with implications for epitranscriptome pathogenesis, Nucleic Acids Res. 49 (2021). D1396-d404.
[28] J.H. Li, S. Liu, H. Zhou, et al., starBase v2.0: decoding miRNA-ceRNA, miRNA-ncRNA and protein-RNA interaction networks from large-scale CLIP-Seq data, Nucleic Acids Res. 42 (2014) D92–D97.
[29] G. Genovese, N.B. Rockweiler, B.R. Gorman, et al., BCFtools/liftover: an accurate and comprehensive tool to convert genetic variants across genome assemblies, Bioinformatics 40 (2024) btae038.
[30] K. Wang, M. Li, H. Hakonarson, ANNOVAR: functional annotation of genetic variants from high-throughput sequencing data, Nucleic Acids Res. 38 (2010) e164.
[31] P.M. Camacho, S.M. Petak, N. Binkley, et al., American association of clinical endocrinologists/american college of endocrinology clinical practice guidelines for the diagnosis and treatment of postmenopausal osteoporosis-2020 update, Endocr. Pract. 26 (2020) 1–46.
[32] D. Bliuc, D. Alarkawi, T.V. Nguyen, et al., Risk of subsequent fractures and mortality in elderly women and men with fragility fractures with and without osteoporotic bone density: the Dubbo Osteoporosis Epidemiology Study, J. Bone Miner. Res. 30 (2015) 637–646.
[33] R.M. Kohli, Y. Zhang, TET enzymes, TDG and the dynamics of DNA demethylation, Nature 502 (2013) 472–479.
[34] J. Kenny, B.H. Mullin, W. Tomlinson, et al., Age-dependent genetic regulation of osteoarthritis: independent effects of immune system genes, Arthritis Res. Ther. 25 (2023) 232.
[35] M. Huang, S. Xu, L. Liu, et al., m6A methylation regulates osteoblastic differentiation and bone remodeling, Front. Cell Dev. Biol. 9 (2021) 783322.
[36] D. Dominissini, S. Moshitch-Moshkovitz, S. Schwartz, et al., Topology of the human and mouse m6A RNA methylomes revealed by m6A-seq, Nature 485 (2012) 201–206.
[37] G.Z. Luo, A. MacQueen, G. Zheng, et al., Unique features of the m6A methylome in Arabidopsis thaliana, Nat. Commun. 5 (2014) 5630.
[38] X. Wang, Z. Lu, A. Gomez, et al., N6-methyladenosine-dependent regulation of messenger RNA stability, Nature 505 (2014) 117–120.
[39] C. Wang, J.A. Inzana, A.J. Mirando, et al., NOTCH signaling in skeletal progenitors is critical for fracture repair, J. Clin. Invest. 126 (2016) 1471–1481.
[40] L.F. Bonewald, G.R. Mundy, Role of transforming growth factor-beta in bone remodeling, Clin. Orthop. Relat. Res. (1990) 261–276.
[41] Y. Yamada, A. Miyauchi, J. Goto, et al., Association of a polymorphism of the transforming growth factor-beta1 gene with genetic susceptibility to osteoporosis in postmenopausal Japanese women, J. Bone Miner. Res. 13 (1998) 1569–1576.
[42] C. Thouverey, J. Caverzasio, Focus on the p38 MAPK signaling pathway in bone development and maintenance, BoneKEy Rep. 4 (2015) 711.
[43] Y. Tanaka, A. Maruo, K. Fujii, et al., Intercellular adhesion molecule 1 discriminates functionally different populations of human osteoblasts: characteristic involvement of cell cycle regulators, J. Bone Miner. Res. 15 (2000) 1912–1923.
[44] Z. Zhou, S. Chen, T. Wu, et al., IGF2BP2, an RNA-binding protein regulates cell proliferation and osteogenic differentiation by stabilizing SRF mRNA, J. Cell. Physiol. 238 (2023) 195–209.
[45] Y. Zou, Z. Li, Y. Zou, et al., An FBXO40 knockout generated by CRISPR/Cas9 causes muscle hypertrophy in pigs without detectable pathological effects, Biochem. Biophys. Res. Commun. 498 (2018) 940–945.
[46] M. Di Monaco, F. Vallero, R. Di Monaco, et al., Prevalence of sarcopenia and its association with osteoporosis in 313 older women following a hip fracture, Arch. Gerontol. Geriatr. 52 (2011) 71–74.
[47] K. Azuma, T. Urano, Y. Ouchi, et al., Glucocorticoid-induced gene tripartite motif-containing 63 (TRIM63) promotes differentiation of osteoblastic cells, Endocr. J. 57 (2010) 455–462.
[48] J.J. Lu, Y. Sun, X. Zhang, et al., [Advances on pentraxin 3 in osteoporosis and fracture healing], Zhong Guo Gu Shang 36 (2023) 393–398.
[49] I. Zofková, P. Nemcikova, P. Matucha, Trace elements and bone health, Clin. Chem. Lab. Med. 51 (2013) 1555–1561.

[50] A. Evilä, J. Palmio, A. Vihola, et al., Targeted next-generation sequencing reveals novel TTN mutations causing recessive distal titinopathy, Mol. Neurobiol. 54 (2017) 7212–7223.
[51] Y. Zhou, C. Zhang, Z. Zhou, et al., Identification of key genes and pathways associated with PIEZO1 in bone-related disease based on bioinformatics, Int. J. Mol. Sci. 23 (2022) 5250.
[52] C. Hernandez-Hernandez, J. Pascual, S. Carlo, et al., Multiple de novo gene variations in a progeroid phenotype case report: Haploinsufficiency mechanisms, AME Case Rep 5 (2021) 40.